Diffraction of Trapped $(CsI)_nCs^+$: The Appearance of Bulk Structure

Stefan Krückeberg, Detlef Schooss, Mathias Maier-Borst, and Joel H. Parks*
Rowland Institute for Science, 100 Edwin H. Land Boulevard, Cambridge, Massachusetts 02142
(Received 25 July 2000)

We report an investigation of $(CsI)_nCs^+$ cluster structures ($n = 30-39$) studied using the recently developed technique of trapped ion electron diffraction. Contributions to diffraction from both rock salt (NaCl) and cesium chloride lattice (CsCl) derived isomeric structures are observed at size $n = 32$. This size can form a closed shell rhombic dodecahedron corresponding to the CsI bulk structure. All other sizes, $n \neq 32$, are dominated by the NaCl structure. Density functional calculations and molecular dynamic simulations identify the presence of a stable CsCl lattice derived structure isomer which is consistent with these results.

PACS numbers: 36.40.Mr, 36.40.Wa

Alkali halide clusters have been the focus of extensive research in cluster physics and chemistry. Mass spectroscopy studies [1–6] of cluster ions $(MX)_nM^+$ and $(MX)_nX^-$ including CsI and CsCl have identified uniquely stable cluster masses for sizes $n \geq 10$ which correspond to cuboids having NaCl structure. These results raise an interesting issue for CsCl and CsI clusters first noted by Martin [7]. Although CsI and CsCl bulk materials have eightfold-coordinated CsCl lattice structure, the mass spectra of these cesium halides are observed to be similar to clusters formed from alkali halide materials having sixfold-coordinated rock salt lattice structure in bulk. This suggests that the emergence of the bulk structure from $(CsI)_nCs^+$ clusters occurs through a size dependent phase transition. This research [8] was motivated by the possibility that electron diffraction of $(CsI)_nCs^+$ clusters could identify cluster structures which help to understand the nature of this transition to bulk structure.

Trapped ion electron diffraction (TIED) is a technique which was developed recently [9] to provide a direct measurement of the dependence of cluster structure on size and temperature. Electron diffraction studies have been performed previously on clusters in supersonic beams [10–13] composed of a distribution of cluster sizes and internal energies. In the measurements described here, it is precisely the ability to mass select and control the cluster temperature which provides the opportunity to observe and interpret the details of size dependent structure. The rf ion trap [14] enables the accumulation of size selected clusters, to collisionally relax the vibrational energy distribution and store the clusters for an adequate time to perform electron diffraction measurements.

The individual components of the experimental apparatus are shown schematically in Fig. 1. The rf trap operates at 300 kHz with an end-cap electrode spacing of 1 cm. The diffraction e-beam of ~0.5 mm diameter traverses the trap through 2 mm apertures in the grounded end-cap electrodes. Diffraction data are obtained for an e-beam energy of 40 keV and beam current of ~400 nA. The primary e-beam is captured in the Faraday cup. The diffracted electrons are detected by an image quality multichannel plate detector forming a pattern on the phosphor screen which is then imaged and recorded on the charge-coupled device (CCD) pixel array. The diffraction pattern has the form of Debye-Scherrer rings similar to powder diffraction as a result of the orientational and spatial disorder of the trapped cluster ions.

Cluster ions are produced by a gas aggregation source [15] in which an oven at ~400 °C evaporates CsI in the presence of He at ~10 °C and ~20 Torr. A current stabilized discharge above the oven aperture produces ions which aggregate to form clusters within the ~1 cm He pathlength to the exit nozzle of the source chamber. Clusters are injected into the trap through an aperture in the ring electrode and the trapped clusters are then

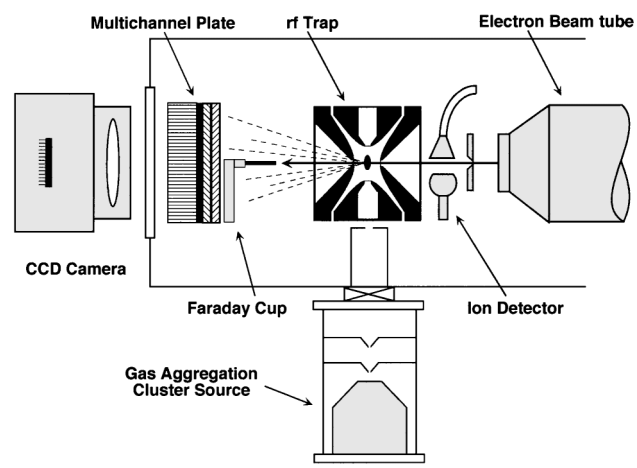

FIG. 1. The diffraction apparatus includes an rf trap, Faraday cup, and microchannel plate detector (MCP) and is structured to maintain a cylindrical symmetry around the electron beam axis. The cluster aggregation source emits an ion beam which is injected into the trap through an aperture in the ring electrode. The e-beam passes through a trapped ion cloud producing diffracted electrons indicated by dashed lines. The primary beam enters the Faraday cup and the diffracted electrons strike the MCP producing a ring pattern on the phosphor screen. This screen is imaged by a CCD camera mounted external to the UHV chamber. The distance from the trapped ion cloud to the MCP is approximately 10.5 cm in these experiment.

 0031-9007/00/85(21)/4494(4)$15.00 © 2000 The American Physical Society

translationally and vibrationally relaxed by a ~10 s exposure to He gas at $\geq 10^{-5}$ Torr. The cluster temperature is established by setting both the trap and He gas temperature at 300 K for these measurements. Prior to diffraction exposures, the He gas is evacuated to a chamber pressure of $\leq 10^{-8}$ Torr to adequately reduce He background scattering. A mass spectrum is obtained by resonantly ejecting trapped ions through the end cap into the ion detector shown in Fig. 1. At ion numbers required for diffraction measurements ($\geq 10^4$ ions) the application of resonant ion excitation [16,17] (SWIFT) is used during ion injection to isolate and trap a single, known cluster size. Inelastic scattering channels were monitored using mass spectra. These spectra indicated that multiply ionized species were the principal loss channel and that vibrational heating of the parent cluster during e-beam exposure was insignificant. Applying SWIFT excitation to the trapped clusters during the diffraction exposure assures that the diffraction data represent a single cluster size.

Diffraction data were obtained from trapped $(CsI)_nCs^+$ for a range of cluster sizes from $n = 30-39$ at a cluster temperature of 300 K. The total scattering intensity is a function of the electron momentum transfer $s = (4\pi/\lambda)\sin(\theta/2)$, where λ is the electron de Broglie wavelength (~0.06 $Å^{-1}$ for 40 keV electrons) and θ is the scattering angle. Figure 2 displays the total scattering intensity data for cluster sizes $n = 30-39$. Peaks in the total intensity correspond to the diffraction pattern rings evident in the CCD camera image shown in the inset. The data clearly indicate that $n = 32$ is different from the data obtained from all other cluster sizes. The phase shift of the peak near $s = 3.5$ $Å^{-1}$ signals a global variation of the cluster structure since the pattern represents interference maxima resulting from summations over all cluster atoms. It is important to point out that the phase shift shown in Fig. 2 for $n = 32$ was completely reproducible, independent of variations in cluster source conditions, variations in trapping conditions, and e-beam exposure. Furthermore, this phase shift was never observed for any other cluster size $n \neq 32$. The similarity of the data shown in Fig. 2 for all $n \neq 32$ demonstrates that the diffraction of clusters in this size range is determined by the overall structural type and not by topological variations within a specific structural type, and also not by cluster sizes within the same structural type. For example, the NaCl and CsCl structural types are easily distinguished by their diffraction patterns. However, the diffraction patterns calculated for a $3 \times 3 \times 7$ parallelepiped $[(CsI)_{31}Cs^+]$ and a $4 \times 4 \times 4$ cubic $[(CsI)_{32}]$, each having the same NaCl structural type but not the same topology, are essentially indistinguishable. The diffraction pattern for a $5 \times 5 \times 3$ $[(CsI)_{36}Cs^+]$ cluster having the same structural type but different size is also indistinguishable from those mentioned above.

The molecular diffraction [18] component was obtained from the total scattering intensity by subtracting a background arising from atomic elastic scattering contributions and contributions from inelastic scattering. This was accomplished using a method [19,20] which relies upon a model of the cluster structure. The resulting molecular diffraction data are then compared with diffraction calculated using this structure model. As the structure model is optimized, the background is recalculated so that the analysis is performed self-consistently.

The structural model for $(CsI)_nCs^+$ clusters was suggested by considering the diffraction intensities in Fig. 2. Mass spectra characterizing the aggregation source and also thermal dissociation measurements of trapped clusters [21] identify $(CsI)_{31}Cs^+$ as a particularly stable cluster which would be expected for a cuboidal ($3 \times 3 \times 7$) NaCl structure. All intensity patterns in Fig. 2 which are identical with $n = 31$ indicate similar structures. The exception occurs for $n = 32$ which suggests the possibility that a different isomer structure may be present for that size. A $(CsI)_{32}Cs^+$ cluster with rhombic dodecahedron geometry forms a closed shell structure at this size which could provide enhanced stability. In addition, this cluster geometry corresponds to the CsCl bulk structure. The presence of this structure was also considered [22] in ion mobility

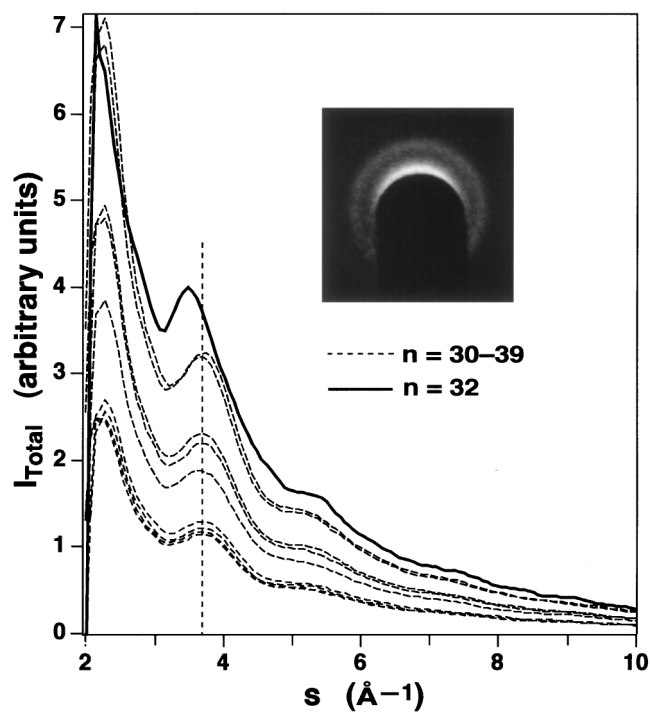

FIG. 2. The inset displays a CCD image of diffraction data obtained after subtracting the electron background contribution. The shadowed area in the pattern results from the Faraday cup. The total diffraction intensity I_{total} vs s ($Å^{-1}$) is obtained by averaging CCD pixel data over several multiple runs. The graph shows experimental data for $(CsI)_nCs^+$ cluster sizes $n = 30, 31, 33, 34, 35, 36, 37, 38,$ and 39 (dashed curves) and $n = 32$ (solid curve). The vertical dashed line which is aligned with peaks for all $n \neq 32$ helps to highlight the phase shift for $n = 32$.

studies of CsI clusters. As a result of these considerations, a model composed of both NaCl and CsCl structure isomers was chosen to represent the ensemble of trapped clusters. A diffraction pattern was calculated for a linear combination of both structures and the fraction of CsCl structure was used as a parameter to optimize the fit to the molecular diffraction data. The effects of cluster temperature were included in the model by using molecular dynamics simulations to estimate Debye-Waller factors in the harmonic approximation. Finally, the finite size of the electron beam introduces an instrumental broadening which was also included in this analysis.

Structural calculations were performed for $n = 31-33$ to determine (a) the presence of a stable CsCl isomer; and (b) the stability against isomerization of such CsCl structures to NaCl structures. The structural optimizations were carried out using the density-functional theory (DFT) [23] method with the Becke-Perdew [24,25] functional as available in the TURBOMOLE [26] program package. In these calculations we employed an ECP-46 (effective core potential for core electrons $1s$-$4d$) which account for scalar relativistic effects.

The isomer for $n = 32$ having a closed shell rhombic dodecahedral geometry was found to be 1.99-eV above the lowest energy structure with NaCl structure ($3 \times 4 \times 5 + 5$) determined by Wales [27] which was used in the DFT structural optimization. These calculations employed a basis set of TZVPP quality (Cs: (7s6p1d/[5s3p1d], I: (4s5p2d1f)/[2s3p2d1f]) [28]. The energy difference between various CsCl and NaCl structures in the case of $n = 31$ and 33 was in the same energy range. Because of the high symmetry of the rhombic dodecahedral structure for $n = 32$, we were able to calculate a vibrational spectrum and verify that this structure represents a stable structure.

Canonical molecular dynamics (MD) simulations using a potential including Born-Mayer repulsion and Coulomb terms were performed with parameters given in Ref. [29]. Starting with the dodecahedral structures from DFT calculations MD simulations showed that only $n = 32$ was stable against isomerization at temperatures $T > 0$ K.

Figure 3(a) displays the molecular diffraction data and the best fits for $(CsI)_nCs^+$ cluster sizes $n = 31$, 32, and 33 at 300 K. The plot at the bottom of Fig. 3 shows the diffraction calculations for both DFT derived isomer structures used in the model. As shown in Fig. 3(b), the broadening of each isomer diffraction pattern introduced by temperature and finite e-beam size seriously reduces the differentiation between these structures. However, the phase shift of the diffraction peak near 3.5 $Å^{-1}$ stands out as the most important signature of the presence of a CsCl structure isomer. The optimum CsCl fractions, f_{CsCl}, derived from fitting data at 300 K are shown in Fig. 4 which also displays the CsCl and NaCl isomers used in the model. This structural isomer model clearly identifies the presence of an isomer population having CsCl structure for $n = 32$, although cluster sizes $n = 30$, 31, 33, and 34 are dominated by NaCl structure.

Although DFT calculations identify a stable, high lying isomer structure of CsCl type for $n = 32$, it is particularly interesting that this structure is observed to account for a population fraction as high as 60% at 300 K. This result is inconsistent with a thermal equilibrium distribution of the NaCl and CsCl isomers at 300 K, assuming the vibrational frequency distributions for each isomer are similar. However, the populations observed could result from relaxation on a larger portion of the potential energy surface (PES) rather than simple excitation of higher lying vibrational levels in a local region about the ground state. We suggest that the possibility for a nonthermal distribution

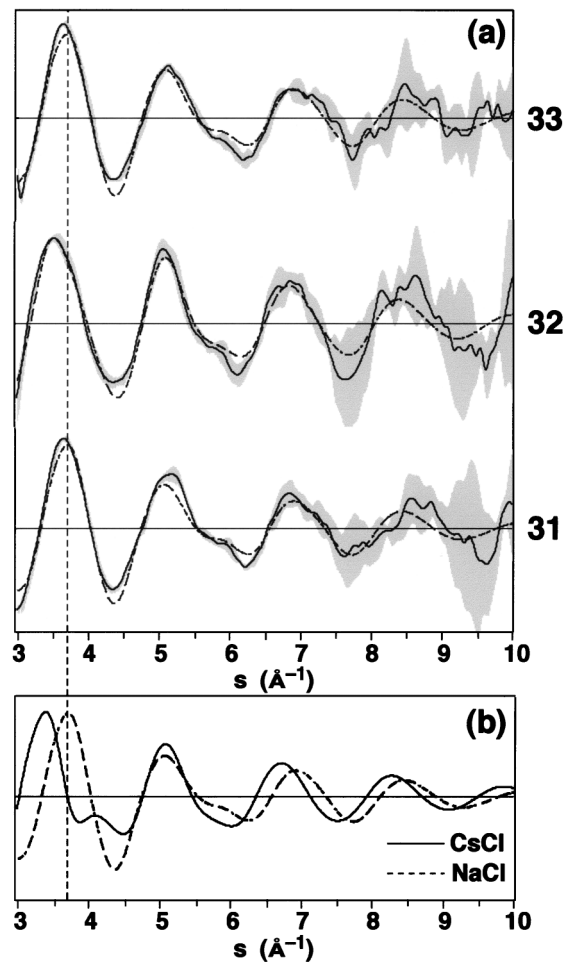

FIG. 3. (a) The graphs compare the experimental (solid curve) and theoretical fit (dashed curve) of the molecular diffraction intensity at 300 K for cluster sizes $n = 31$, 32, 33 averaged over multiple runs. The experimental curve is obtained from I_{total} shown in Fig. 2 after subtracting the diffraction background signal. The standard deviation $\pm 1\sigma$ is shown for each size (light gray band) characterizing the run to run reproducibility. (b) This graph shows the molecular diffraction intensity for the model NaCl and CsCl structures including broadening by vibrational motion at 300 K and by finite e-beam size. The vertical dashed line which is aligned with the NaCl peak in (b) helps to highlight the phase shift for $n = 32$ in (a).

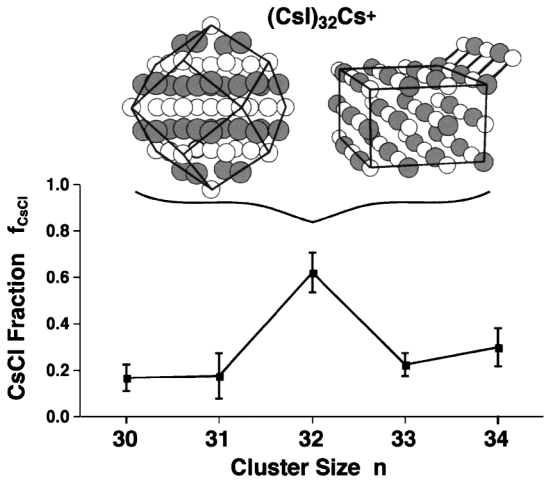

FIG. 4. The fraction of CsCl structure, f_{CsCl}, present in the molecular diffraction at 300 K for cluster sizes $n = 30-34$ is shown. The cluster structures used in the model are shown with solid lines as guides for the eye.

arising from relaxation downward on the PES (as opposed to thermal heating) is consistent with these diffraction observations. Diffraction measurements are being performed at both higher and lower temperatures to study the dynamics responsible for these results.

Diffraction data of $(\mathrm{CsI})_n\mathrm{Cs}^+$ clusters have been described here by a model which suggests an interesting possibility for realizing the structural transition from clusters to bulk material. Although the dominant structure for $(\mathrm{CsI})_n\mathrm{Cs}^+$ may be found experimentally to correspond to NaCl structures for most sizes, there are unique sizes associated with closed atomic shells for which this does not occur, such as $n = 32$. At these sizes, the bulk CsCl structure can become a dominant isomer even though it does not have the lowest energy as a result of the stability gained by its compact, rhombic dodecahedral closed shell structure. This infers that similar results may be found for higher closed shell clusters ($n = 87, 184, \ldots$). As the cluster size continues to increase, a range will eventually be reached for which the dynamics responsible for the bulk structure [30,31] dominate and the CsCl structures will become lower in energy than NaCl structures. The possibility this cluster size range is currently being investigated.

This research was fully supported by The Rowland Institute for Science.

*Author to whom correspondence should be addressed. Electronic address: parks@rowland.org

[1] J.E. Campana, T.M. Barlak, R.J. Colton, J.J. Decorpo, J.R. Wyatt, and B.I. Dunlap, Phys. Rev. Lett. **47**, 1046 (1981).
[2] R. Pflaum, P. Pfau, and E. Recknagel, Surf. Sci. **156**, 165 (1985); R. Pflaum, K. Sattler, and E. Recknagel, Chem. Phys. Lett. **138**, 8 (1987).
[3] E.C. Honea, M.L. Homer, P. Labastie, and R.L. Whetten, Phys. Rev. Lett. **63**, 394 (1989).
[4] Y.J. Twu, C.W.S. Conover, Y.A. Yang, and L.A. Bloomfield, Phys. Rev. B **42**, 5306 (1990).
[5] P. Labastie, J.M. L'Hermite, Ph. Poncharal, and M. Sence, J. Chem. Phys. **103**, 6362 (1995).
[6] R.L. Whetten, Acc. Chem. Res. **26**, 49 (1993).
[7] T.P. Martin, J. Chem. Phys. **69**, 2036 (1978).
[8] J.H. Parks, in Proceedings of the Third International Symposium on Theory of Atomic and Molecular Clusters, Humboldt-Universität Berlin, Berlin, Germany, 1999 (unpublished).
[9] M. Maier-Borst, D.B. Cameron, M. Rokni, and J.H. Parks, Phys. Rev. A **59**, R3162 (1999).
[10] B.G. De Boer and G.D. Stein, Surf. Sci. **106**, 84 (1981); A. Yokozeki and G. Stein, J. Appl. Phys. **49**, 2224 (1978).
[11] J. Farges, M.F. Feraudy, B. Raoult, and G. Torchet, Surf. Sci. **106**, 95 (1981); J. Farges, B. Raoult, and G. Torchet, J. Chem. Phys. **59**, 3454 (1973).
[12] J.W. Hovick and L.S. Bartell, J. Phys. Chem. B **102**, 534 (1998); L.S. Bartell, Chem. Rev. **86**, 491 (1986).
[13] D. Reinhard, B.D. Hall, D. Ugarte, and R. Monot, Phys. Rev. B **58**, 4917 (1998); D. Reinhard, B.D. Hall, P. Berthoud, S. Valkealahti, and R. Monot, Phys. Rev. B **55**, 7868 (1997).
[14] J.H. Parks, S. Pollack, and W. Hill, J. Chem. Phys. **101**, 6666 (1994); J.H. Parks and A. Szöke, J. Chem. Phys. **103**, 1422 (1995).
[15] M. Maier-Borst, dissertation, Universität Konstanz, 1997.
[16] S. Guan and A.G. Marshall, Int. J. Mass Spectrom. Ion Process. **157/158**, 5 (1996); A.G. Marshall, T.-C.L. Wang, and T.L. Ricca, J. Am. Chem. Soc. **107**, 7893 (1985).
[17] R.K. Julian, Jr. and R.G. Cooks, Anal. Chem. **58**, 14 (1993); M.H. Soni and R.G. Cooks, Anal. Chem. **66**, 2488 (1994).
[18] *Stereochemical Applications of Gas-Phase Electron Diffraction,* edited by I. Hargittai and M. Hargittai (VCH, New York, 1988).
[19] P. D'Antonio, C. George, A.H. Lowrey, and J. Karle, J. Chem. Phys. **55**, 1071 (1971).
[20] M. Dantus, S.B. Kim, J.C. Williamson, and A.H. Zewail, J. Phys. Chem. **98**, 2782 (1994).
[21] Experimental data to be presented elsewhere.
[22] P. Löffler, Ph.D. thesis, Universität Konstanz, 1999.
[23] K. Eichkorn, O. Treutler, H. Öhm, M. Häser, and R. Ahlrichs, Chem. Phys. Lett. **240**, 283 (1995).
[24] A.D. Becke, Phys. Rev. A **36**, 3098 (1988).
[25] J.D. Perdew, Phys. Rev. B **33**, 8822 (1986).
[26] R. Ahlrichs, M. Bär, H. Horn, and C. Kömel, Chem. Phys. Lett. **162**, 165 (1989).
[27] D.J. Wales (private communication).
[28] K. Eichkorn, F. Weigand, O. Treutler, and R. Ahlrichs, Theor. Chem. Acc. **97**, 119 (1997).
[29] D.O. Welch, O.W. Lazareth, G.J. Dienes, and R.D. Hatcher, J. Chem. Phys. **64**, 835 (1976).
[30] P. Jemmer, M. Wilson, P.A. Madden, N.C. Pyper, and P.W. Fowler, J. Chem. Phys. **111**, 2038 (1999); P.A. Madden and M. Wilson, Chem. Soc. Rev. **25**, 339 (1996).
[31] N.C. Pyper and P. Popelier, J. Phys. Condens. Matter **9**, 471 (1997); N.C. Pyper, Chem. Phys. Lett. **220**, 70 (1994).